HIGH-LIFT INVESTIGATIONS ON SOME SMALL ASPECT RATIO WINGS

ICAS-80-12.3

H. Körner
Deutsche Forschungs- und Versuchsanstalt für
Luft- und Raumfahrt, Institut für Entwurfsaerodynamik
Braunschweig

Abstract

An experimental investigation of the flow on some unconventional small aspect ratio wings at high angle of attack is given. The investigation comprises force and flow field measurements as well as flow visualization by oil-flow, wool tuft in the wake and smoke injections on backward and forward swept and hybrid wings. The study shows that a stable flow behaviour can be generated for a number of different planforms.

For these cases aerodynamic coefficients (C_L, C_D, C_M) are presented. The flow visualization gives a deeper insight into the phenomenology of the flow.

1. Introduction

Vortex flow is of great importance for small aspect ratio wings, especially for delta-wings and wings with strakes. The separated vortices originating from the leading edges generate additional lift and give high α_{CLmax} with a regular, steady flow field. This type of flow has already been investigated to a large extent especially for delta-wings and wings with strakes (1) - (8).

The flow on a delta-wing is characterized by 4 regimes

- attached flow all over the wing at angles of attack near $\alpha \approx 0^o$.
- concentrated vortices originating from the leading edge at angles of attack between 5^o and 20^o to 40^o - this depends on leading edge sweep.
- vortex formation with more or less burst vortices above 20^o to 40^o.
- separated flow without primary structure and unsteady character at very high angle of attack.

Methods on the basis of empirism and potential flow modelization have been developed which allow the evaluation of the aerodynamic derivatives as far as they are connected with lift effects for the first and the second regime (9) - (12). Some more sophisticated approaches in addition allow the calculation of the pressure distribution (13) - (14). All these methods fail when break-down occurs; this means that regime 3 and 4 are still beyond theoretical treatment although some theoretical work has been done in this field (15) - (17).

Since separated vortex flow is a powerful means to generate higher lift and to have a stable behaviour of the flow up to high angles of attack, the question arises, whether such type of flow can be generated for alternative configurations as

- wings with forward swept leading edges
- hybrid wings with forward and backward swept leading edges
- wings with backward and forward swept trailing edges.

If this is valid, the scope of tentative wing configurations could be extended.

In order to find answers to the posed problem, experimental investigations on a number of unconventional wings of small aspect ratio have been performed. These investigations included:

- 3-component force measurements
- surface flow visualization by a petroleum-aluminium mixture, similar to oil-flow visualization
- visualization of the vortices by smoke injection
- visualization of the wake flow by wool tufts fixed on a grid - for some special cases.
- flow field measurements in the wake - for some special cases.

These investigations have been done to find quantitative results for selected unconventional configurations but also to get an insight into the phenomenology of the flow. This point has to be stressed.

In the following chapters the test set-up will be described roughly and the results will be presented.

2. Test set-up

The main part of the investigations has been performed in the 2.8 m x 3.6 m Low Speed Windtunnel of DFVLR-WT-NW Braunschweig (18). This is a closed circuit windtunnel with an open test section having a maximum speed of 75 m/s. The force measurements and the flow visualization work have been done in this windtunnel. Figure 1 shows the test set-up in the open test-section of the windtunnel. The force measurements have been performed at a wind-speed of 40 m/s resp. 25 m/s for the higher angles of attack due to limitations of the strain-gauge balance. For the very high angles of attack a change of the support-system had to be made. The surface flow visualization and the wool tuft

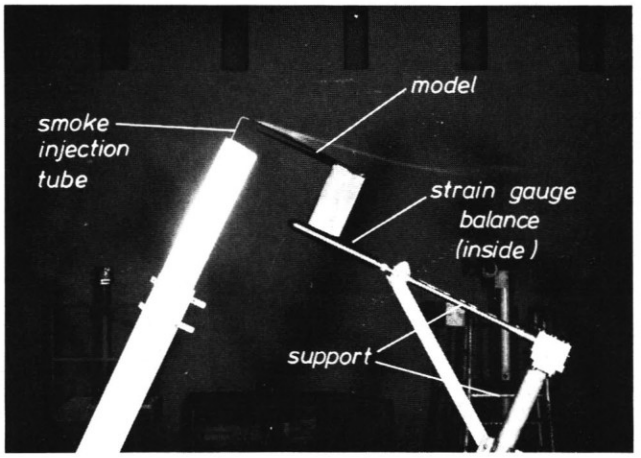

FIGURE 1. Test set-up in the 2,8 m x 3,6 m Low Speed Windtunnel of DFVLR Braunschweig

investigations have been done at a wind-speed of 40 m/s and the smoke visualization with 13 m/s.

The flow field measurements have been performed in the 3 m x 3 m Low Speed Windtunnel of DFVLR-WT-NW Göttingen (19). This windtunnel which is simular to the Braunschweig windtunnel is equipped with a set-up for flow field measurements. The wind-speed for these investigations was also 40 m/s.

Since the effects to be investigated are closely related to the planform geometry of the models, these will be described in detail when discussing the results in chapter 3 to 5. Here some general remarks on the models will be made. All models are made of steel-plates of 2.5 mm thickness with sharp edges of 15° if not indicated otherwise. These sharp edges are achieved by slanting the lower side. This leads to a small negative camber of the mean line.

The main planform data of the wings investigated are given in table 1. The aspect ratio varies from 0.7 to 3 and the planform taper from 0 to 3.42.

3. Wings with forward swept leading edges

In order to get an insight in the behaviour of wings with forward swept leading edges at high angle of attack a series of wings has been tested (figure 2). Basic wing is K 3 with a forward sweep of 50°. One varying form originating from this is K 2 with a higher forward sweep of 60°. In the other line of variation the forward sweep remains 50° and the wing is formed having a more realistic planform-taper with highly swept trailing edges. As reference wings K 5 and K 6 are measured in the inserve manner as K 11 and K 12.

Figure 3 shows the results for the 3-component force measurements for wings with leading edge sweep variation

Wing	Aspect Ratio	Plan-form-Taper	Remarks
K 2	1,27	3,42	
K 3	1,53	2,67	
K 4	1,11	0,135	Leading edge droop, rounded leading edge, see fig. 20
K 5	2,57	0	
K 6	1 43	0,290	
K 7	2,1	0,184	
K 8	0,91	0,150	Leading edge droop, rounded leading edge, see fig. 20
K 9	0,7	—	
K 10	1,11	0,135	K 4 inverse
K 11	2,57	0	K 5 inverse
K 12	1,43	0,290	K 6 inverse
K 16	3,0	0	
K 17	1,74	0	
K 21	0,92	0,203	
K 22	1,35	1	

TABLE 1. Main geometric parameters of the wings

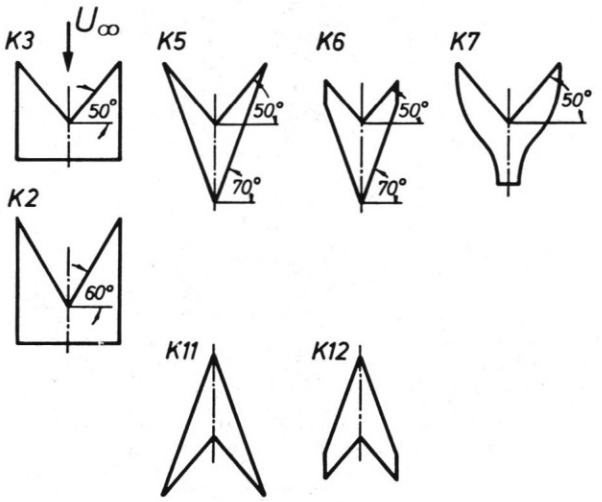

FIGURE 2. Wing series 1

(K 2, K 3). As can be seen from the C_L-α diagramm K 3 (50°) shows up to 12° a linear behaviour with a severe degradation of the lift-slope at approximately 20°, followed by a steep ascent to C_{Lmax} = 1.0 near α = 30°.

The wing K 2 shows a moderate nonlinear behaviour up to the suggested vortex-burst at 15°. The first peak in C_L is attained at 22° with C_L = 0.75, then the lift curve declines to a relative minimum value in C_L

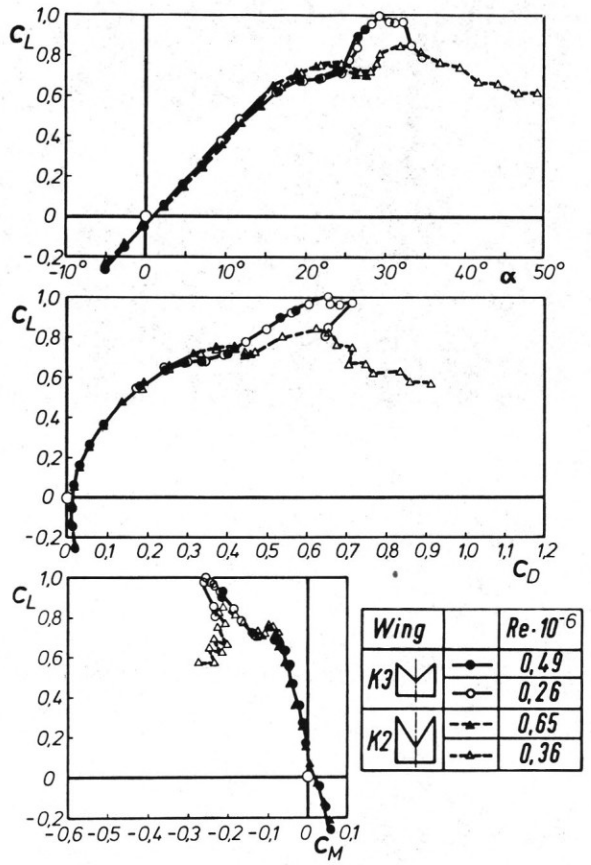

FIGURE 3. 3-component force measurements for K 2 and K 3

at 27° and has a second maximum at 32° with c_L = 0.85.

What are the effects dominating this behaviour? This will be demonstrated by flow visualization.

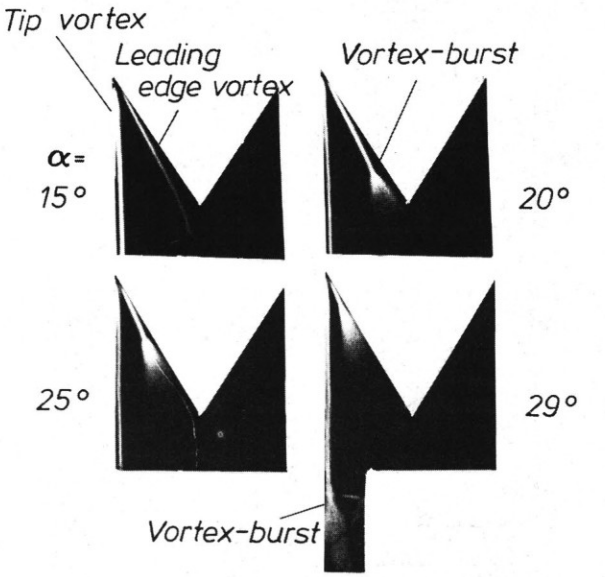

FIGURE 4. Flow visualization by smoke - K 2

Figure 4 shows a visualization of the vortices by smoke. As can be seen there exist two vortices on a wing-half originating from the tip leading edge

- one following the leading edge and turning in streamwise direction near midspan
- a second one following the tip edge.

At an angle of attack of 15° the leading edge vortex is still well concentrated. With growing angle of attack the location of vortex-burst moves in upstream direction. At α = 29° the burst-location has almost reached the tip. In contrast to this the tip vortex remains stable and vortex-burst first reaches the trailing-edge beyond α = 29°.

In addition to this, figure 5 shows some surface flow pictures with the location of the vortices indicated on one wing-half. The formation of the leading edge vortex can be seen quite clear. In front of this main vortex a secondary vortex system builds up at the leading edge which feeds into a zone with complicated flow-behaviour in the midspan region. This zone increases up to α = 15°. At higher angle of attack this zone is taken over by the bursting leading edge vortex. This bursting vortex together with the counter-rotating tip vortex gives a regular structure to the flow field up to α = 30°. Beyond this value the flow becomes highly unsteady.

Although besides the tip vortex an inward vortex exists, the tip vortex is dominating in the wake. This can be seen quite clear from a wool tuft investigation which was performed at 0.9 span behind the wing. Figure 6 shows that for an angle of attack of 20° the tip vortices are still strong whereas the inward vortices have already decomposed. This can also be seen from flow field measurements. Figure 7 shows the flow field perpendicular to the streamwise direction 0.2 maximum chord in front of the trailing edge. Also here the inward vortex has already burst while the tip vortex is still strong.

Let's now turn over to somewhat more realistic wings with planform-taper less than 1. Figure 8 shows a comparison of three forward swept wings with the same leading edge sweep of 50°. Wing K 6 originates from K 5 by cutting up the tips. Results of force measurements for similar wings have been given by (9). All three wings show a nearly linear behaviour up to approximately α = 10°. Beyond this value the lift slope decreases continuously up to C_{Lmax} near 30°. At higher angles of attack above 40° the curves show a saw-tooth form which has been reproduced several times even when changing the integration-time of the values. In this region the flow has an unsteady character. It cannot be excluded that some spurious effects may produce these results.

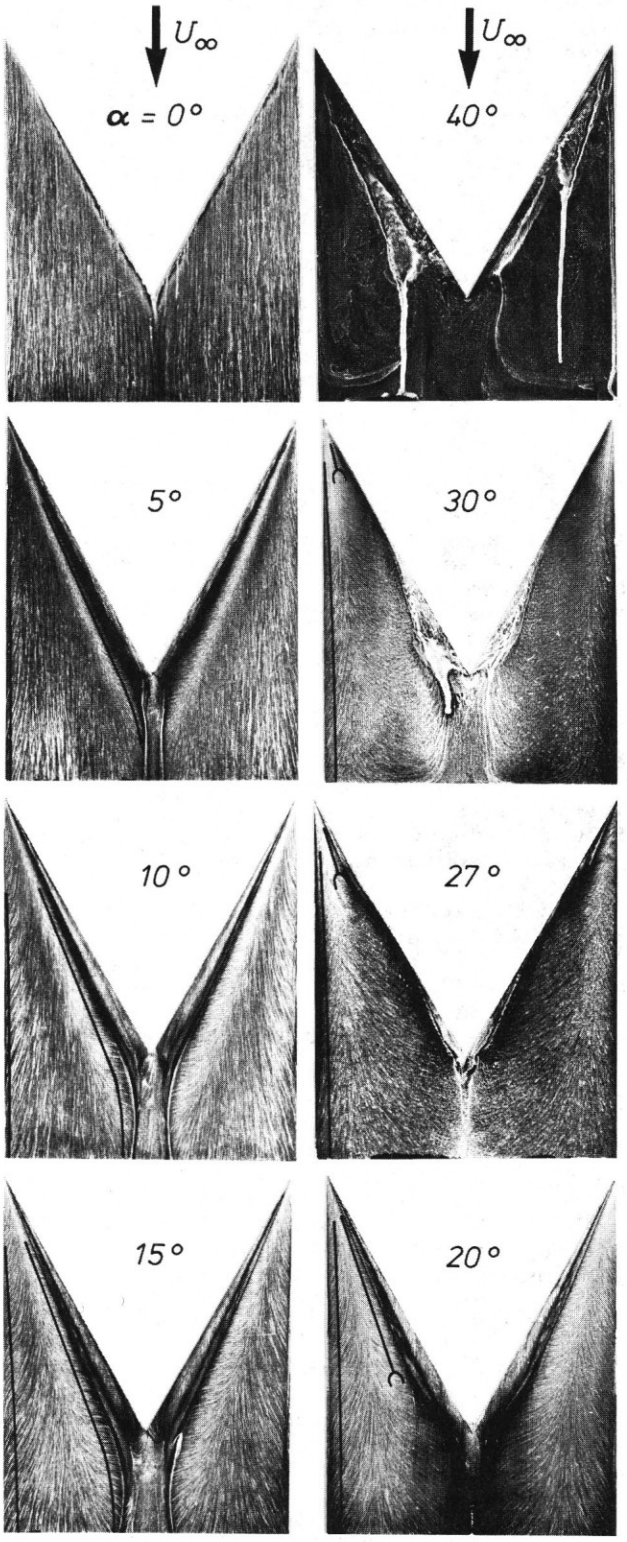

FIGURE 5. Surface flow visualization - K 2

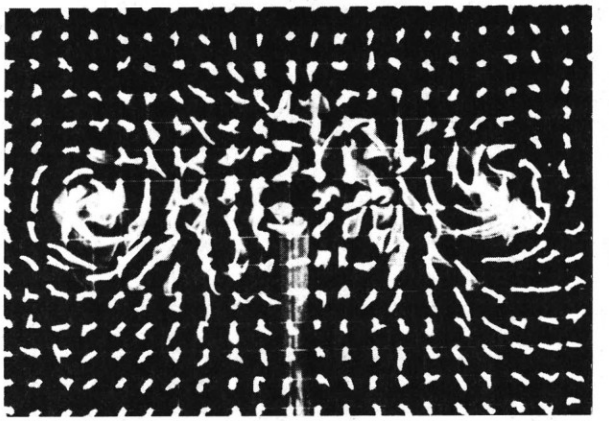

FIGURE 6. Wake visualization by wool tuft - K 2 ($\alpha = 20^{o}$)

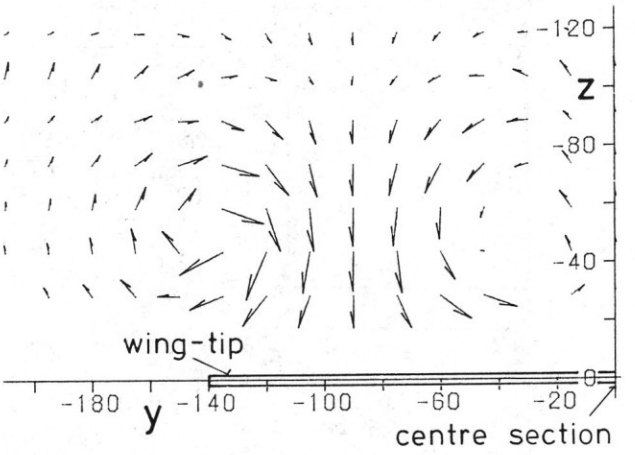

FIGURE 7. Flow field measurements K 2 ($\alpha = 20^{o}$)

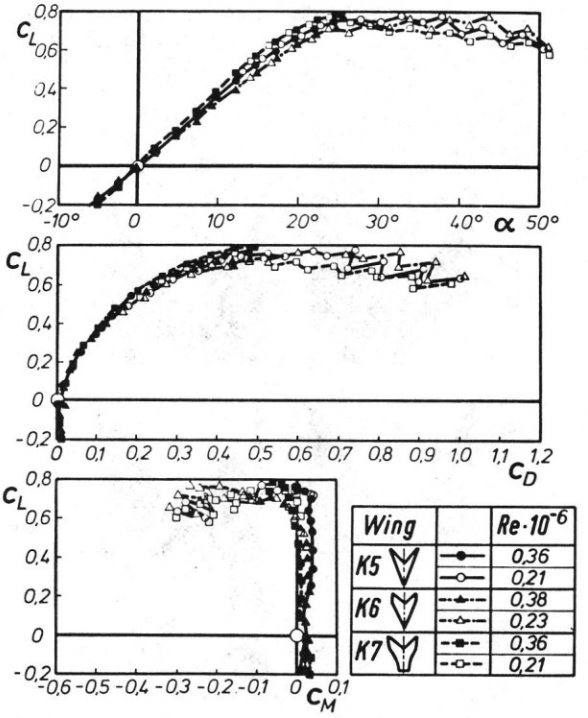

FIGURE 8. 3-component force measurements for K 5, K 6 and K 7

The drag behaviour exhibits no peculiarities but it is worthwhile to mention that the wing K 5, which has a somewhat higher aspect ratio than the others is not the best one with respect to drag. Obviously the pointed tips are not favorable. The pitching moment shows a linear behaviour up to $C_L = 0.7$.

Now, what about the behaviour of the flow. To clarify this, surface flow visualization for wing K 5 is shown on figure 9. The

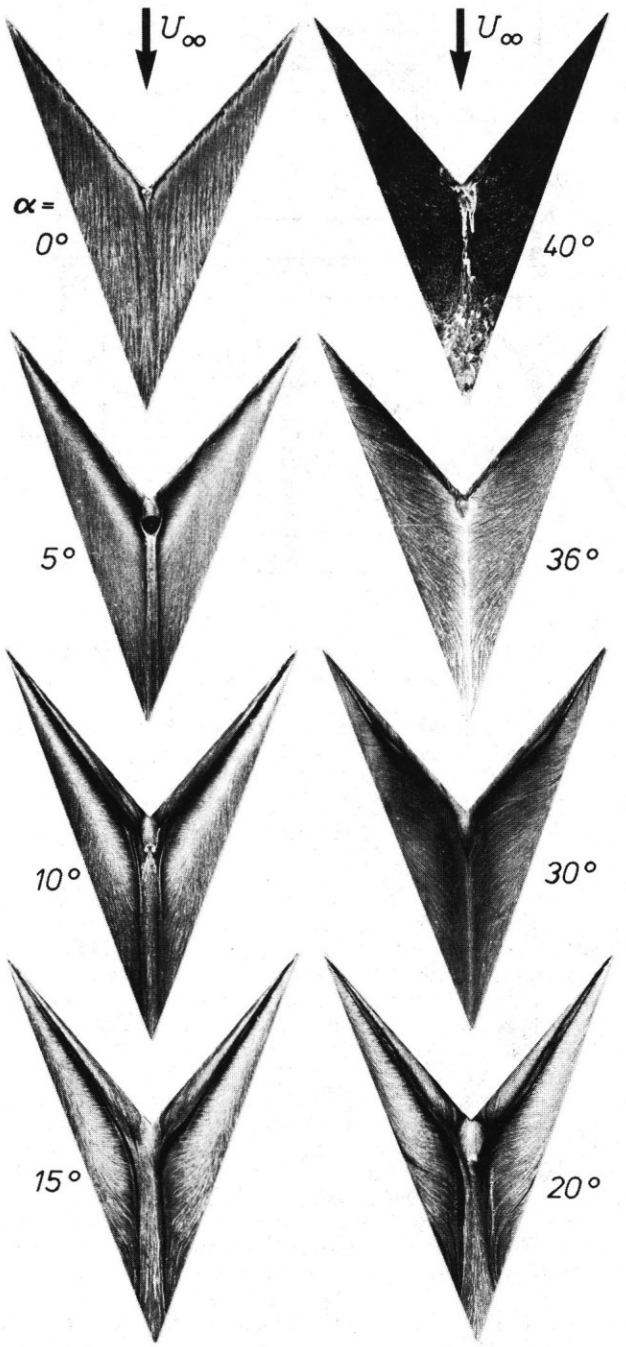

FIGURE 9. Surface flow visualization - K 5

main features can be summarized as follows:

- regular flow field up to $\alpha = 36^\circ$.
- formation of a leading edge vortex at approximately $\alpha = 5^\circ$
- formation of a secondary vortex system in front of the primary vortex
- midspan-region with secondary effects, which may cause additional drag
- vortex-burst begins at the trailing edge between 10° and 15°. This can be seen from smoke visualization
- collapse of the midspan secondary flow region between 20° and 30°
- at 40° unsteady separated flow.

Smoke visualization shows that there exists a tip vortex which is located outside the wing-planform.

A comparison of the flow pattern of the wings K 5, K 6, K 7 with the inverse flow case for K 5 and K 6 is given in figure 10 for $\alpha = 30^\circ$. The planforms show a regular flow behaviour except K 6 and K 7. The flow on the wings K 5, K 6 and K 7 is dominated by totally burst vortices. In contrast to this, in the reverse flow cases the flow field is still governed by concentrated vortices which break down near the trailing edge. This will lead to a higher efficiency.

A comparison of the force results for K 5 and K 11 (figure 11) shows that K 5 only has a very weak nonlinear behaviour in the lift up to $\alpha = 10^\circ$, whereas in the reverse flow case (K 11, arrow-wing) this point is reached at the much higher angle of 24°. C_{Lmax} is attained for both configurations between 30° and 40° where the lift curve has a plateau type. As to C_{Lmax}, K 11 is superior to K 5 with 1.12 versus 0.8. The drag polars show that even at low lift coefficients the wing K 11 is superior to K 5. The pitching moment is approximately the same.

The comparison of wing K 6 and K 12 shows similar tendency. Therefore the results for K 12 are omitted here.

The results achieved from this study can be summarized as follows: vortices from swept forward leading edges

- create a regular steady flow field up to high angles of attack
- bring a moderate nonlinear lift-contribution.

In comparison with similar swept back wings (inverse flow case) it can be seen that swept forward planforms have some disadvantages as smaller C_{Lmax} and higher drag.

This is due to

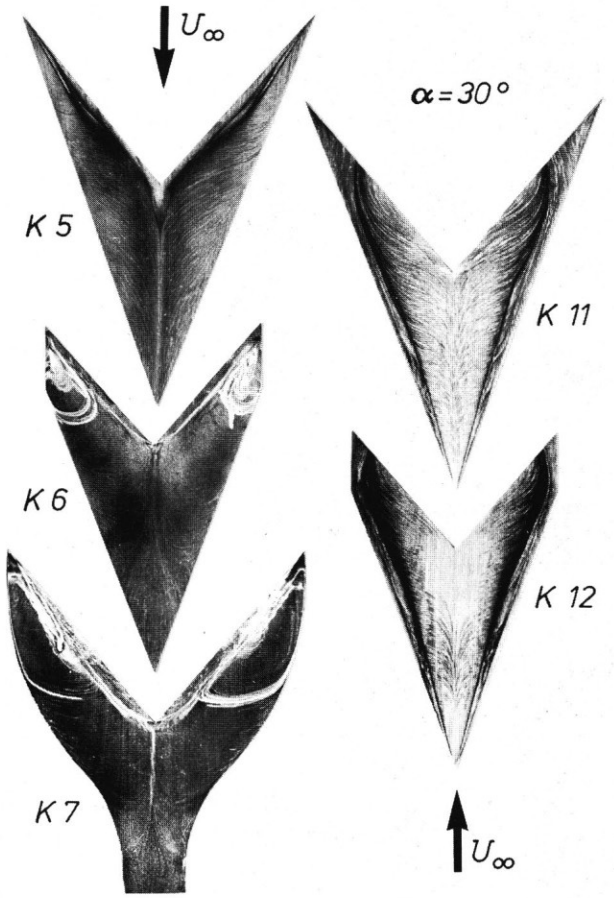

FIGURE 1o. Surface flow visualization - K 5, K 6, K 7, K 11 and K 12 (α = 30°)

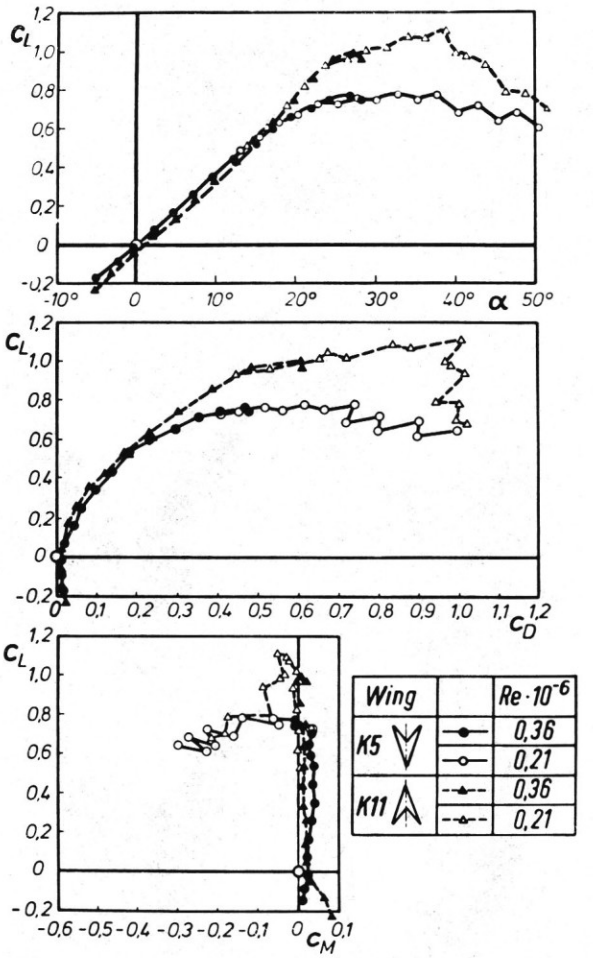

FIGURE 11. 3-component force measurements for K 5 and K 11

- the relatively moderate forward sweep of the leading edges that can be achieved. This leads to premature vortex break-down.
- the lack of further high energy air fed into the vortex in midspan
- counter-rotating vortices merging in the midspan region so that
  - -- each vortex reduces the effectiveness of the other
  - -- with increasing α a growing area of dead air flow is created in the midspan region and
  - -- vortex break-down is influenced by this and obviously occurs earlier than in the swept back case.

  This difficulty could perhaps be overcome by inserting a body in midspan position.

Besides this another point deteriorates the performance of a swept forward configuration with vortex flow a priori. This is the fact that the leading edge vortex counter-rotates to the tip vortex, which leads to additional drag.

4. Hybrid wings with combined forward and backward swept leading edges

The next step now is to combine forward and backward sweep to preserve the good basic behaviour of backward sweep with some additional benefit from forward sweep. To get an insight into the behaviour of such hybrid configurations two derivatives (K 17, K 22) of a delta-wing (K 21) have been designed (figure 12). K 17 has a forward swept planar winglet and K 22 is generated from K 21 by omitting the inward front part of the delta-wing, thus having a wing with forward and backward sweep of both φ = 70°. The fourth configuration investigated is a biplane consisting of a forward upper delta-wing combined with a rearward lower swept forward wing (K 9).

The results of the force measurements for K 17, K 21 and K 22 are given in figure 13. All wings have a nonlinear lift curve which is strongest for the clean delta-wing. This wing has a C_{Lmax} of 1.3 at α = 35°, wing

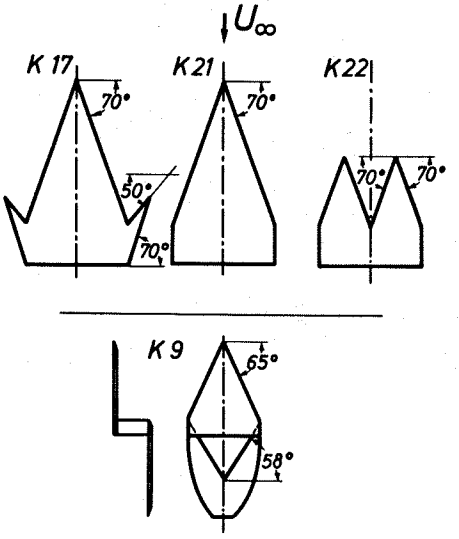

FIGURE 12. Wing series 2

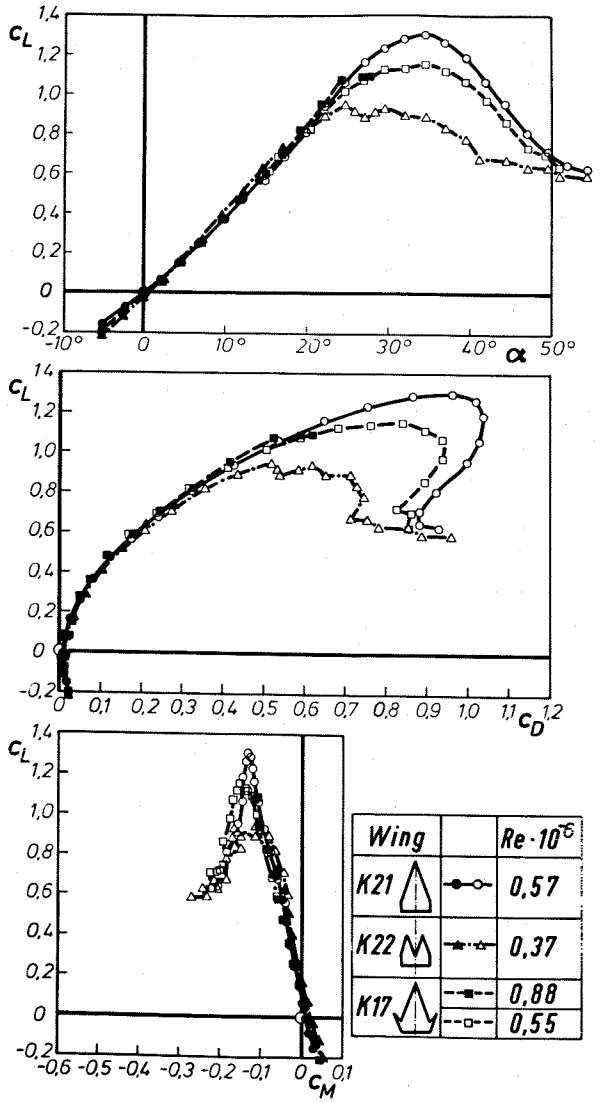

FIGURE 13. 3-component force measurements for K 17, K 21 and K 22

K 17 - the delta-wing with tip extension 1.15 at the same angle of attack whereas K 22 is below 1 at $\alpha = 25^o$. In the post-stall region the clean delta-wing shows a smooth behaviour up to $\alpha = 60^o$. This is also valid for the drag polar. As to drag at small lift coefficients there is no large discrepancy between the wings but also here the clean delta-wing shows a slightly better behaviour. The pitching moment is for all wings nearly linear up to C_{Lmax}.

Let's have a look on the flow phenomena by studying some surface flow pictures. Figure 14 gives photos of the wings K 17, K 21 and K 22 for $\alpha = 15^o$ and 25^o. The delta-wing shows the typical well-known flow field with a reattachment region in the midspan area, a strong primary vortex originating from the leading edge and a secondary vortex area. Even in the high angle of attack case ($\alpha = 25^o$) vortex-burst has not yet occurred.

The delta-wing with tip-extension shows similar behaviour for the main wing. On the swept forward extension a leading-edge vortex builds up with a rather large secondary vortex which feeds dead air into the junction region. At $\alpha = 25^o$ the vortex has obviously burst and the strong vortex of the main wing dominates the junction region. Further clarification can be given by figure 15 where the smoke visualization shows that the tip vortex begins to burst at even small angles of attack. At $\alpha = 25^o$ the tip vortex is totally broken down. Obviously the strong vortex of the main wing stimulates the break-down of the counter-rotating tip vortex.

The third wing treated in figure 14 is wing K 22. Each half of the wing shows the typical behaviour of a single delta-wing. Nevertheless it can be seen quite clear, that for $\alpha = 15^o$ there is a large junction region with dead air. Vortex-burst has already reached the trailing edge, while the tip-vortex is still strong. This can be confirmed by wool tuft visualization of the wake flow 0.9 span behind the wing for $\alpha = 20^o$ (figure 16). As can be seen the tip vortices are still strong whereas the inward region exhibits an irregular flow behaviour with unsteady effects.

This study shows that

- when vortices interfere, the weaker one is dominated by the stronger one. In the case K 17, the main vortex induces an upwash in the region of the planar winglet. This leads to a premature break-down of the vortex

- forward sweep even at the same degree of sweep does not give as good performance as backward sweep. The reasons for this are summarized in chapter 3.

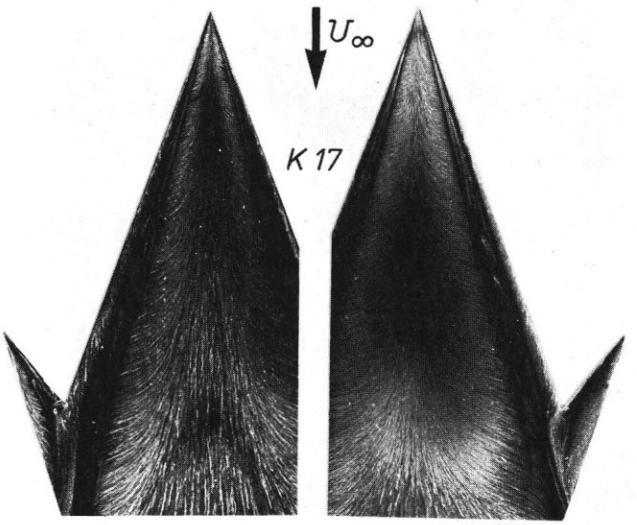

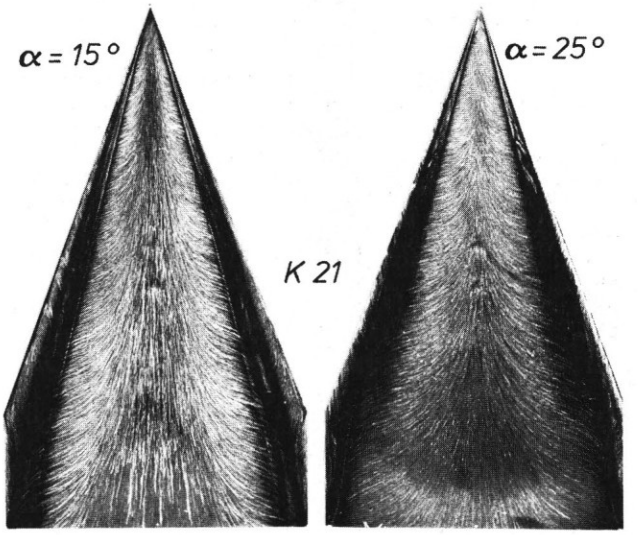

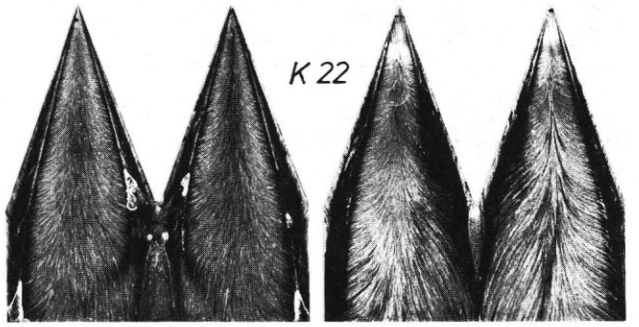

FIGURE 14. Surface flow visualization - K 17, K 21 and K 22

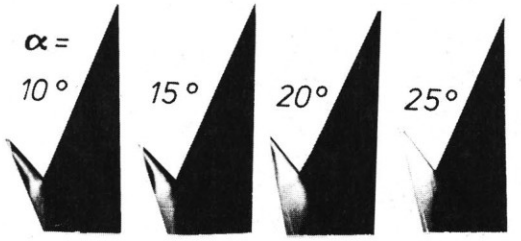

FIGURE 15. Flow visualization by smoke - K 17

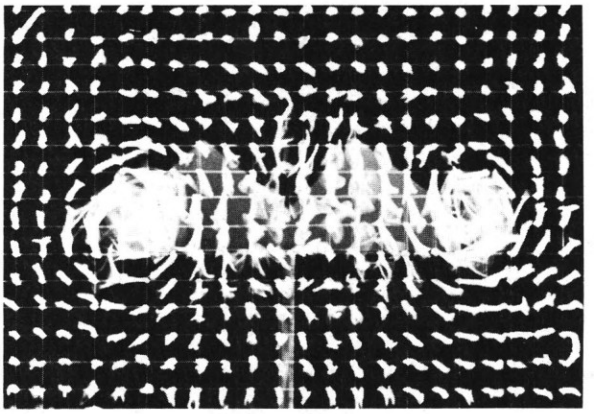

FIGURE 16. Wake flow visualization by wool tuft - K 22 ($\alpha = 20^{\circ}$)

Besides these planar configurations a more complex nonplanar biplane has been investigated. From the results of the force measurements in figure 17 can be seen that a

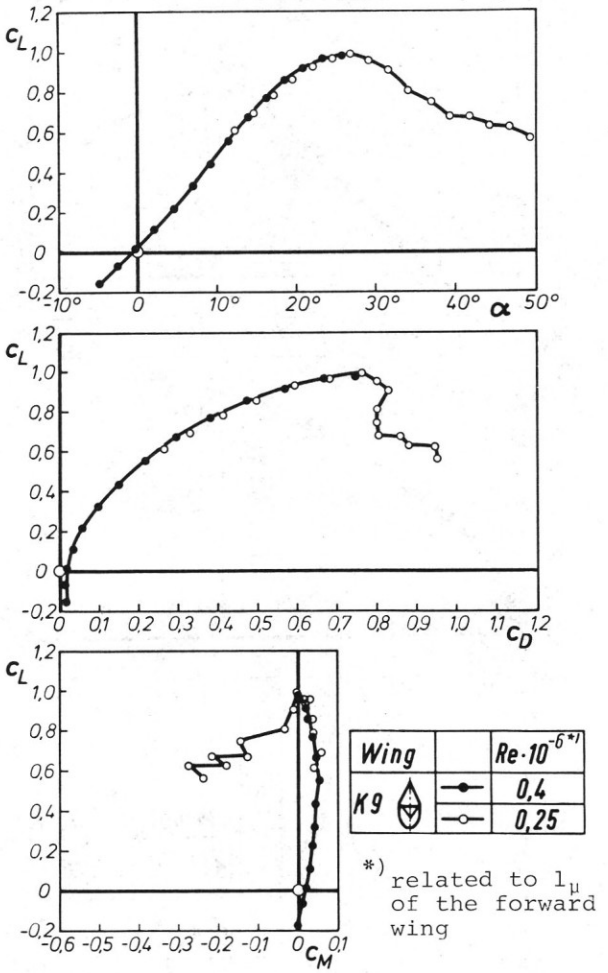

*) related to l_μ of the forward wing

FIGURE 17. 3-component force measurements for K 9

good nonlinear behaviour can be achieved. The maximum lift occurs between 25° and 30°. The post-stall is as smooth as for a single delta-wing.

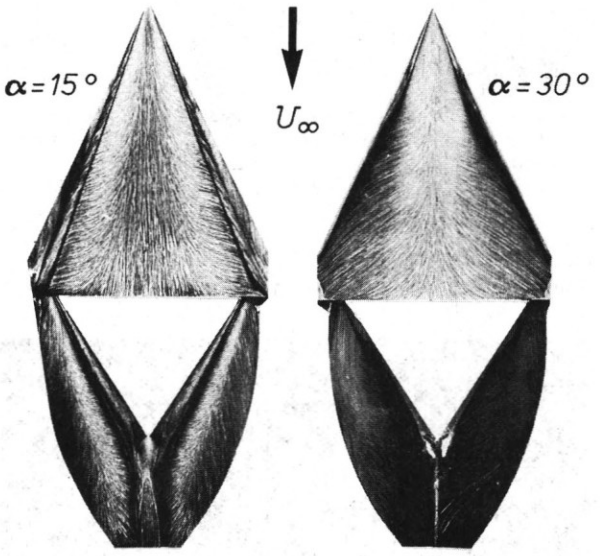

FIGURE 18. Surface flow visualization - K 9

Figure 18 shows a surface flow picture for $\alpha = 15^{\circ}$ and 30° which exhibits quite clear the well organized flow on upper and lower wing. This is valid up to high angles of attack.

5. Wings with forward and backward swept trailing edges

The question arises whether there exist concentrated vortices originating from the trailing edge. If they exist, can they be used to create a regular steady flow field? Do they generate nonlinear effects? These questions shall be investigated using a third series of wings (figure 19). Wing K 4 is an

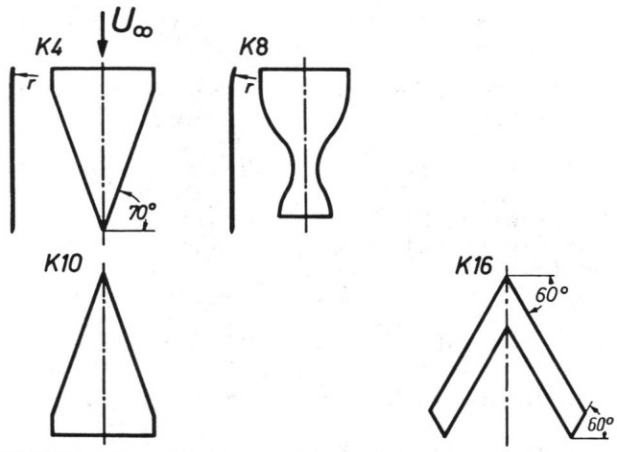

FIGURE 19. Wing series 3

inverse delta-wing with nose droop and rounded leading edge. K 8 has a reverse gothic form with an appendix. K 10 is the inverse K 4 used as reference. K 16 is a 60° swept back wing with constant chord except near the tip.

The idea of the geometry of wing K 4 is to get attached flow in the inward part up to moderate angles of attack. At the tips then will build up a vortex, which is to be hoped to follow the trailing edge line and forcing down the midspan flow up to high angles of attack. The philosophy of K 8 is similar to this.

Looking at the force measurements (figure 20) K 10 (delta-wing) exhibits a

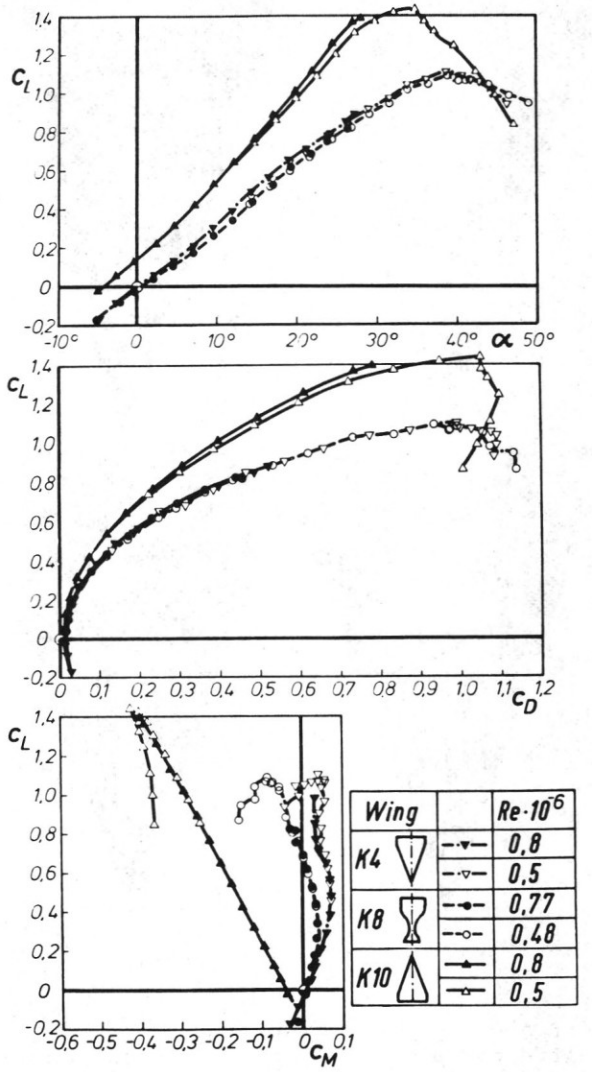

FIGURE 20. 3-component force measurements for K 4, K 8 and K 10

strong nonlinear behaviour up to $\alpha = 24^{\circ}$ with a C_{Lmax} of more than 1.4 at $\alpha = 34^{\circ}$. K 4 and K 8 in contrast have only a small but perceivable nonlinear behaviour in the range between $\alpha = 5^{\circ}$ and 20°. C_{Lmax} is for both wings approximately 1.1 and occurs at a very high angle of attack near 40°. The further post-stall behaviour is smooth and gives higher C_L-values than the delta-wing.

The drag polars for the unconventional configurations are inferior to that of the delta-wing. The pitching moment does not show a good linear behaviour for K 4 and

K 8 while the delta-wing has a linear trend up to high C_L-values.

Now, what are the informations that flow visualization can give us? Figure 21 gives

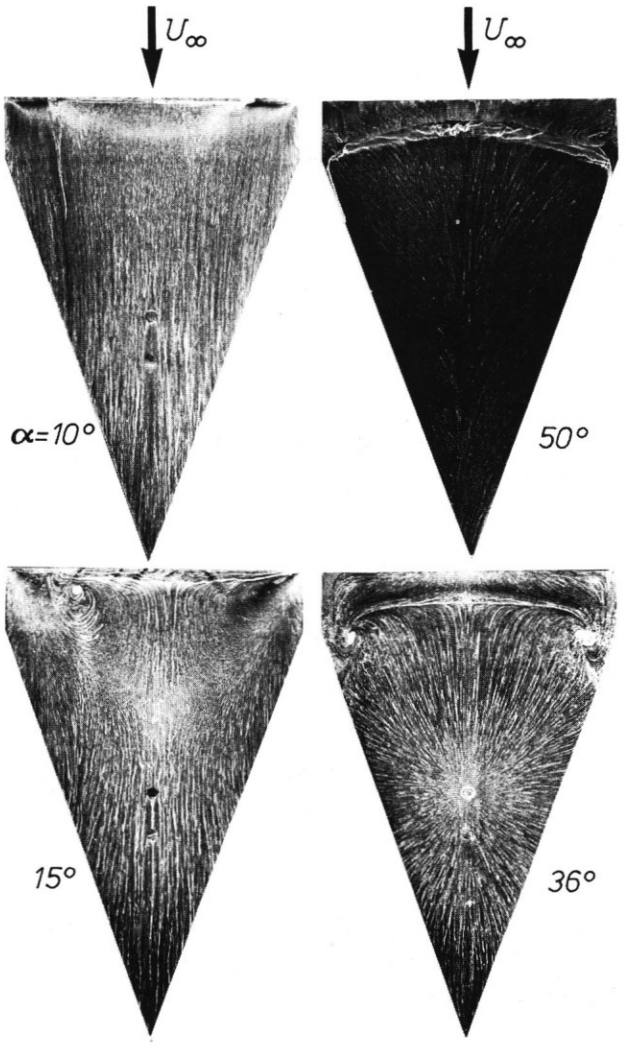

FIGURE 21. Surface flow visualization - K 4

surface flow pictures for wing K 4 at different angles of attack. It can be seen that for

- α up to 10° the flow is attached all over the wing. Near the tip the formation of a weak vortex can be seen.
- $\alpha = 15^\circ$: the flow separates immediately behind the leading edge and reattaches at 1/3 of the chord in midspan. The tip vortex has become stronger; in spite of this its influence on the rear part of the wing can be neglected.
- $\alpha = 20^\circ - 40^\circ$ the separation-line has moved a bit backwards and ends in two vortices, the influence of the tip vortices disappears and the reattachment-point is located in the mid of the wing.
- $\alpha = 50^\circ$: now reattachment has been shifted beyond the trailing edge and the upper side of the wing is totally exhibited to reverse flow.

Further information can be drawn from wool tuft visualization in the wake. Figure 22 shows that at $\alpha = 20^\circ$ there

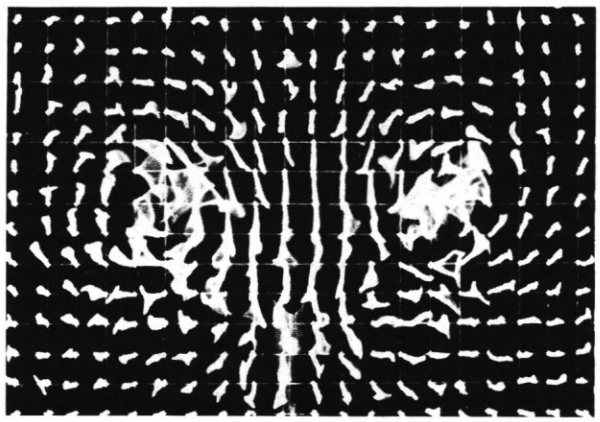

FIGURE 22. Wake flow visualization by wool tuft - K 4 ($\alpha = 20^\circ$)

is a pair of vortices. Although these vortices seem to be burst they create a regularly formed inward region with a smooth downward flow. Unsteady effects seem to be of minor importance.

The results of these investigation are:

- the vortex from the tip has only a moderate influence on the wing surface flow up to 15°.
- nevertheless a well formed relatively stable flow is achieved up to 40°.
- some nonlinear effects can be observed.

Following the idea of vortices originating from the trailing edge, an alternative configuration has been investigated.

This is a swept wing of aspect ratio 3 with constant chord and 60° sweep. Figure 23 shows the surface flow at $\alpha = 15^\circ$. Besides the main vortex, which is bursting before it reaches the trailing edge, a trailing edge vortex builds up. This becomes stronger with rising α.

6. Conclusions

Besides wings with backward leading edge sweep alternative configurations exist as e.g. forward swept wings where concentrated vortices can be used to

- create regular steady flow fields up to high angles of attack
- create some favorable nonlinear effects.

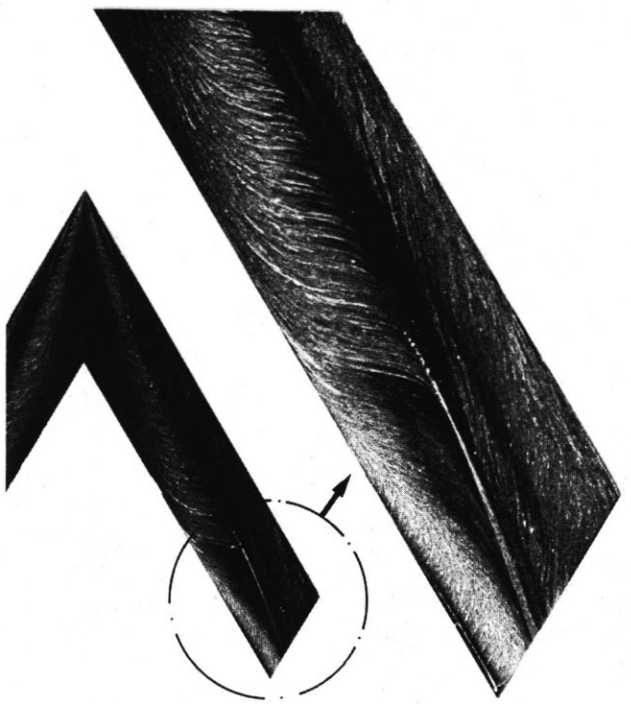

FIGURE 23. Surface flow visualization - detail of the flow on the rear part of the wing K 16 ($\alpha = 15^{\circ}$)

Nevertheless the delta-wing seems to be best suited for the use of favorable effects of concentrated vortex separation. Detrimental effects of swept forward configurations are

- reduced effectiveness of vortices which counter-rotate in midspan

- premature vortex break-down caused by counter-rotating vortices, the lack of further high energy air fed into the vortex in midspan and an extended dead air region in midspan.

All this leads to a reduced efficiency.

It has been found that also trailing edge vortices can rearrange separated flow to a certain extent. Beyond this flow patterns may occur which are not dominated by a leading or trailing edge vortex but nevertheless show a relatively smooth flow behaviour.

Acknowledgement

The author thanks Ing. W. Hastreiter and Dipl.-Phys. A. Kühn for the technical performance of the windtunnel test.

References

(1) Küchemann, D.: The Aerodynamic Design of Aircraft. Pergamon Press 1978

(2) Poisson-Quinton, Ph.: Slender wings for civil and military aircraft. Isreal Journal of Technology 16, 1978, pp.97-131

(3) Smith, J.H.B.: A review of separation in steady, three-dimensional flow AGARD-CP 168, 1975, pp. 31-1 to 31-17

(4) Moss, G.: Some UK research studies of the use of wing-body strakes on combat aircraft configurations at high angles of attack. AGARD-CP 247, 1978, pp. 4-1 to 4-19

(5) Staudacher, W.; Laschka, B.; Poisson-Quinton, Ph. and Ledy, J.P.: Aerodynamic characteristics of a fighter type configuration during and beyond stall. AGARD-CP 247, 1978, pp. 8-1 to 8-15

(6) Hummel, D.: On the vortex formation over a slender wing at large angles of incidence. AGARD-CP 247, 1978, pp. 15-1 to 15-17

(7) Mirande, J.; Schmitt, V. and Werlé, H.: Système tourbillonnaire à l'extrados d' une aile en flèche à grande incidence. AGARD-CP 247, 1978, pp. 12-1 to 12-18

(8) Luckring, J.M.: Flow visualization studies of a general research fighter model employing a strake-wing concept at subsonic speeds. NASA-TM 80057, 1979

(9) Lamar, J.E., Luckring, J.M.: Recent theoretical developments and experimental studies pertinent to vortex flow aerodynamics - with a view towards design. AGARD-CP 247, 1978, pp. 24-1 to 24-31

(10) Belotserkovskii, S.M.: Calculation of the flow about wings of arbitrary planform for a wide range of angles of attack. RAE Lib. Transl. No 1433, 1970

(11) Rehbach, C.: Numerical investigation of leading-edge vortex for low-aspect ratio thin wings. AIAA Journ. 14, 1976, pp. 253-255

(12) Schröder, W.: Die Berechnung der nichtlinearen Beiwerte von Flügeln mit kleinem und mittlerem Seitenverhältnis nach dem Wirbelleiterverfahren. DFVLR-FB 78-26, 1978

(13) Johnson, F.T.; Tinico, E.N.; Lu, P. and Epton, M.A.: Recent advances in the solution of three-dimensional flows over wings with leading edge vortex separation. AIAA Paper 79-0282, 1979

(14) Hoeijmakers, H.W.M.; Bennekers, B.: A computational model for the calculation of the flow about wings with leading edge vortices. AGARD-CP 247, 1978, p.. 25-1 to 25-11

(15) Das, A.: Zum Anschwellen aufgerollter Wirbelflächen und Aufplatzen des Wirbelkerns bei schlanken Tragflügeln. Z. Flugwiss. 15, 1967, pp. 355-362

(16) Wedemeyer, E.H.: Stable and instable vortex separation. AGARD-CP 247, 1978, pp. 13-1 to 13-10

(17) Wilson, J.D.: Calculation of vortex breakdown locations for flow over delta wings. J. Aircraft 14, 1977, p. 1020-1022

(18) Trienes, H.: Der Normalwindkanal der Deutschen Forschungsanstalt für Luft- und Raumfahrt (DFL) in Braunschweig. Z. Flugwiss. 12, 1964, pp. 135-142

(19) Riegels, F.W., Wuest, W.: Der 3 m-Kanal der AVA, Z. Flugwiss. 9, 1961, pp. 222-228